Backbone ^{1}H, ^{13}C, and ^{15}N Assignments and Secondary Structure of Bovine Low Molecular Weight Phosphotyrosyl Protein Phosphatase†

Ming-Ming Zhou,‡ Timothy M. Logan,‡ Yves Thèriault,‡,§ Robert L. Van Etten,*,∥ and Stephen W. Fesik*,‡

Pharmaceutical Discovery Division, Abbott Laboratories, Abbott Park, Illinois 60064, and Department of Chemistry, Purdue University, West Lafayette, Indiana 47907-1393

Received December 23, 1993; Revised Manuscript Received March 4, 1994®

ABSTRACT: Phosphotyrosyl protein phosphatases play an important role in mediating cellular signal transduction; yet three-dimensional structures of this important class of proteins have not been reported. We present the sequence-specific ^{1}H, ^{13}C, and ^{15}N backbone assignments for the low molecular weight bovine heart phosphotyrosyl protein phosphatase (BHPTPase) (157 residues, 17 900). The assignments were obtained from a combination of double- and triple-resonance multidimensional NMR experiments. From these assignments, the secondary structure of BHPTPase was determined from an analysis of NOE patterns, $^{3}J_{HNH\alpha}$ coupling constants, $^{13}C^{\alpha}$ and ^{13}CO chemical shifts, and amide ^{1}H exchange rates. BHPTPase was found to consist of a four-stranded parallel β-sheet (residues K6–C12, W39–A45, Y87–M91, and K112–L116), four α-helices (residues I21–D32, R58–G67, S94–N104, and D135–R157), and one stretch of 3_{10}-helix (residues K79–F85). The secondary structure is characteristic of the $\beta\alpha\beta$ structural motif. The secondary structure elements identified in this study are consistent with previous chemical and mutagenesis studies of BHPTPase structure.

Protein tyrosine phosphorylation and dephosphorylation are critical to many physiological events in the cell, including control of signal transduction for cellular growth and differentiation (Hunter & Cooper, 1985; Yarden & Ullrich, 1988). *In vivo*, tyrosine phosphorylation levels reflect a balance between the action of protein tyrosine phosphatases (PTPases)[1] and protein tyrosine kinases (PTKases). Overexpression of protein tyrosine kinases can cause cell transformation (Yarden & Ullrich, 1988), and it has been suggested that protein tyrosine phosphatases may function as tumor suppressor genes (Fischer et al., 1991). Like tyrosine kinases, PTPases constitute a large family of enzymes that can be divided into two classes: one subfamily, which includes CD45, LAR, and PTP 18 (Guan & Dixon, 1990), is characterized by having both extracellular receptor and transmembrane regions, with one or more cytoplasmic catalytic domains. The second subfamily consists of soluble cytosolic proteins containing a single catalytic domain. This class can be further subdivided according to their functional roles and subcellular locations, i.e., SH2-containing SHPTP-1 (Yi et al., 1992), cytoskeletal PTPMEG1 (Gu et al., 1991), and a dual-specificity PTPase VH1 (Guan et al., 1991), as well as the more recently discovered nuclear PTPases, PAC-1 (Rohan et al., 1993) and dPTP61F (McLauglin & Dixon, 1993).

Within the class of cytosolic PTPases, a group of low molecular weight cytoplasmic protein tyrosine phosphatases may also be important in mediating intracellular protein tyrosine dephosphorylation and thus play a role in regulating intracellular signal transduction pathways that control diverse cellular processes. These enzymes have been isolated from a variety of mammalian tissues (Heinrikson, 1969; Taga & Van Etten, 1982; Chernoff & Li, 1985; Oakada et al., 1986; Boivin et al., 1987; Waheed et al., 1988; Zhang & Van Etten, 1990; Manao et al., 1992). Amino acid and cDNA sequencing of several of these enzymes has revealed a high degree of sequence homology (Camici et al., 1989; Wo et al., 1992a,b; Dissing et al., 1991; Manao et al., 1992). In most organisms, there appear to be two forms of these PTPases. The two human isoenzymes are apparently derived from a single gene by an alternative splicing of the primary RNA transcript (Lazaruk et al., 1993). The amino acid sequences of the two isoenzymes are homologous except in the region of residues 40–73, where roughly half of the residues are different. The bovine PTPase that is the subject of the present study is highly homologous (94% identical) to the electrophoretically slow isoenzyme of human "red cell" acid phosphatase. Recent results utilizing mRNA hybridization experiments have shown that in fact this enzyme is expressed in all human tissues and is not unique to red cells (Wo et al., 1992b). Both isoenzymes have been shown *in vitro* to possess phosphatase activity with different specificities for phosphotyrosine-containing protein or peptide substrates, including tyrosine-phosphorylated angiotensin, tyrosine kinase p40, erythrocyte band 3, IgG, and EGF receptor (Chernoff & Li, 1985; Boivin & Galand, 1986; Waheed et al., 1988; Ramponi et al., 1989; Zhang & Van Etten, 1990). More recently, it has been demonstrated that overexpression of the bovine low molecular weight PTPase in NIH/3T3 fibroblasts inhibits normal and oncogene v-*erb*B-transformed cell growth (Ruggiero et al., 1993).

Although the low molecular weight PTPases exhibit no general sequence homology with receptor-like PTPases (such as CD45) or other known cytosolic nonreceptor PTPases (such as the human placental PTP 1B), all PTPases contain sequence similarity in the enzyme active-site region, including a number of critical catalytic residues conserved in all PTPases. Direct

† The research at Purdue University was supported by USDHHS Research Grant GM 27003.

* Authors to whom correspondence should be addressed.

‡ Abbott Laboratories.

§ Present address: Ontogen Corp., 2325 Camino Vida Roble, Carlsbad, CA 92009.

∥ Purdue University.

® Abstract published in *Advance ACS Abstracts,* April 1, 1994.

[1] Abbreviations: C′, carbonyl carbon; HSQC, heteronuclear single quantum coherence; NOE, nuclear Overhauser enhancement; NOESY, nuclear Overhauser enhancement spectroscopy; PAO, phenylarsine oxide; PTPase, protein tyrosine phosphatase; PTKase, protein tyrosine kinase; TOCSY, total correlation spectroscopy; TPPI, time-proportional phase incrementation.

0006-2960/94/0433-5221$04.50/0

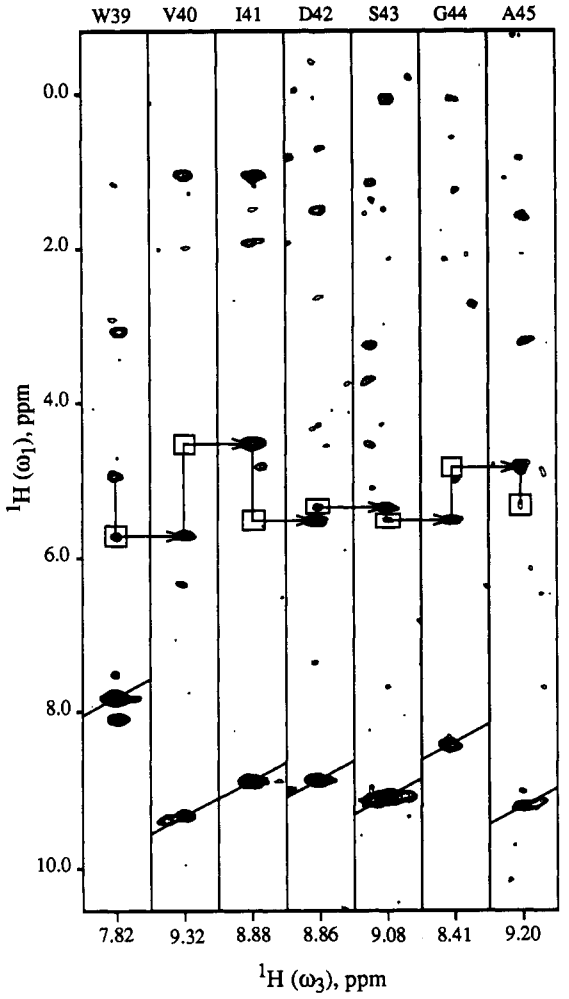

FIGURE 1: ^{1}H(ω_1), ^{1}H (ω_3) cross sections of a 50-ms 3D NOESY-HSQC spectrum of a β-strand region of [U-^{15}N]BHPTPase extracted at the ^{15}N chemical shifts (ω_2) of residues W39–A45. The intraresidue $^1H^N$–$^1H^\alpha$ cross-peaks that were observed in a 3D TOCSY-HSQC spectrum of [U-^{15}N]BHPTPase are indicated by boxes. Interresidue $^1H^N_{(i)}$–$^1H^\alpha_{(i-1)}$ NOEs used in sequential assignments are marked by arrows.

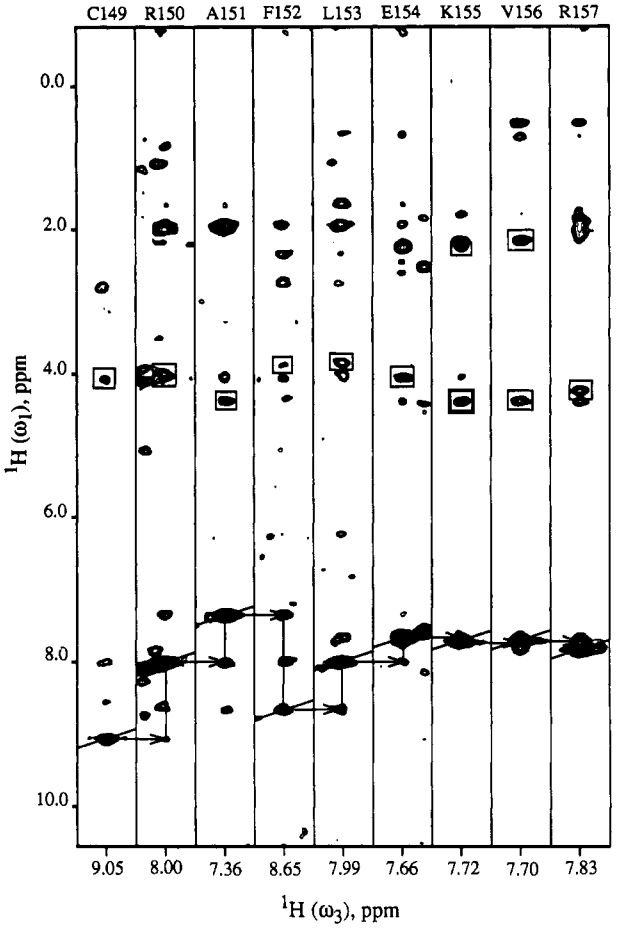

FIGURE 2: ^{1}H(ω_1), ^{1}H(ω_3) cross sections of a 50-ms 3D NOESY-HSQC spectrum of an α-helical region of [U-^{15}N]BHPTPase extracted at the ^{15}N chemical shifts (ω_2) of residues C149–R157. $^1H^N$–$^1H^\alpha$ cross-peaks that were observed in a 3D TOCSY-HSQC spectrum of [U-^{15}N]BHPTPase are indicated by boxes. Sequential $^1H^N$–$^1H^N$ connectivities are indicated by arrows.

observation of the stoichiometrically trapped phosphocysteine intermediate using ^{31}P NMR provided conclusive evidence in support of a cysteine residue as the enzymatic nucleophile in PTPase catalysis (Wo et al., 1992a). Subsequently, site-directed mutagenesis studies of bovine PTPase revealed that C12 is the enzyme nucleophile (Davis et al., 1992, 1994a; Cirri et al., 1993). In addition, mutation of R18 produces completely inactive protein. More recently, mutagenesis, kinetic, and ^{1}H NMR spectroscopic studies of human and bovine PTPases demonstrated that H72 is located at the enzyme active site and may be involved in interacting with the substrate phosphate moiety, although it is not essential for catalysis (Zhou et al., 1993; Davis et al., 1994b). Further detailed studies of function, catalytic mechanism, and substrate specificity of PTPases have been hampered by the lack of structural information on this family of proteins. To date, no three-dimensional structure is available for any PTPase, including this group of low molecular weight PTPases.

In this paper, we report the ^{1}H, ^{13}C, and ^{15}N backbone resonance assignments for 147 of 151 non-prolyl residues of bovine heart low molecular weight PTPase. Using these assignments, we have determined the secondary structure of BHPTPase from NOEs, $^3J_{HNH\alpha}$ coupling constants, $^{13}C^\alpha$ and ^{13}CO chemical shifts, and amide proton exchange rates. This study represents the first step toward the elucidation of the 3D solution structure of a protein tyrosine phosphatase with the goal to further our understanding of this interesting class of proteins.

EXPERIMENTAL PROCEDURES

Protein Expression, Purification, and NMR Sample Preparation. Recombinant bovine heart protein tyrosine phosphatase was prepared as previously described (Wo et al., 1992a; Zhou, 1993). Uniformly ^{15}N and ^{15}N/^{13}C labeled BHPTPases were prepared by growing the bacteria in M9 minimal medium using $^{15}NH_4Cl$ as the sole nitrogen source or $^{15}NH_4Cl$ and [$^{13}C_6$]glucose as the sole nitrogen and carbon sources, respectively. Selectively ^{15}N amino acid labeled BHPTPase proteins were prepared using procedures similar to those reported previously (Hoffman & Spicer, 1991; Zhou, 1993). NMR samples (1–2 mM enzyme) contained 100 mM sodium phosphate in a 90% H_2O/10% D_2O solution at pH 5.0. The isotopically ^{15}N-labeled amino acids, $^{15}NH_4Cl$, and [$^{13}C_6$]glucose were purchased from either Isotec Inc. or Cambridge Isotope Laboratories.

NMR Spectroscopy. Some initial spectra were collected on a Varian VXR-600 spectrometer. Subsequent NMR spectra were collected at 303 K on either a Bruker AMX500 or AMX600 NMR spectrometer. Quadrature detection in the indirectly detected dimensions was accomplished using the States–TPPI method (Marion et al., 1989a). The raw

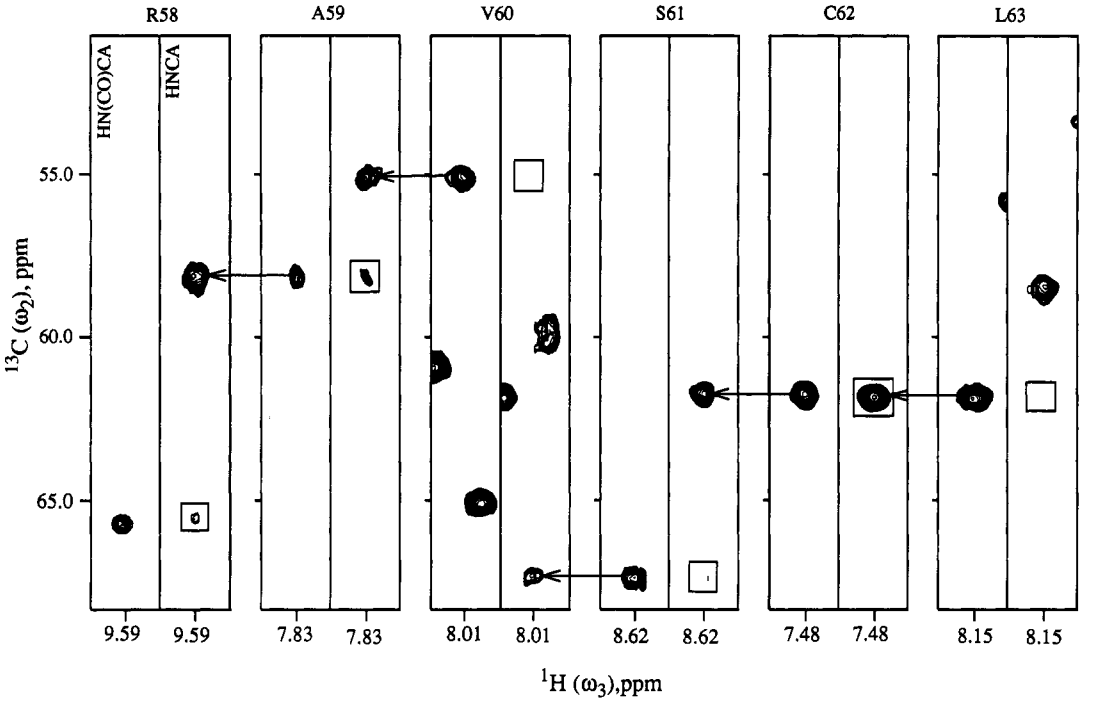

FIGURE 3: Selected $^{13}C^{\alpha}(\omega_2)$, $^{1}H^{N}(\omega_3)$ cross sections of the 3D HNCA and 3D HN(CO)CA spectra of [U-^{15}N,^{13}C]BHPTPase extracted at the $^{15}N(\omega_1)$ chemical shifts of the amino acids shown at the bottom of the spectra. The position of the interresidue $^{1}H^{N}_{(i)}$–$^{15}N_{(i)}$–$^{13}C^{\alpha}_{(i-1)}$ correlation peaks in the HNCA spectrum are indicated by boxes. The intraresidue $^{1}H^{N}_{(i)}$–$^{15}N_{(i)}$–$^{13}C^{\alpha}_{(i)}$ correlation peaks in the HNCA spectrum are marked by arrows.

data were transformed and analyzed on Silicon Graphics computers using in-house-written software.

Two-dimensional ^{1}H–^{15}N heteronuclear single quantum coherence (HSQC) (Bodenhausen & Ruben, 1980) spectra of uniformly ^{15}N-labeled and selectively ^{15}N amino acid labeled BHPTPase samples were recorded using a spin-lock purge pulse for water suppression (Messerle et al., 1989).

Three-dimensional HNCA (Ikura et al., 1990) and HN(CO)CA (Bax & Ikura, 1991) experiments were collected on the AMX600 under identical conditions with 18 × 48 × 2048 complex points using sweep widths of 2656 Hz (^{13}C, t_1), 1947 Hz (^{15}N, t_2), and 10,000 Hz (^{1}H, t_3), respectively. For both experiments, a total of 64 scans per increment were recorded for a total acquisition time of 120 h for the two experiments. The ^{1}H carrier was set to the water frequency, and the ^{13}C and ^{15}N carriers were set to 59.6 and 116.3 ppm, respectively. Solvent suppression and the removal of spectral artifacts were afforded by gradients (Bax & Pochapsky, 1992). Using previously described approaches (Olejniczak & Eaton, 1990), the complex data were extended in the two indirect dimensions using linear prediction prior to apodization and Fourier transformation. Final data set sizes were 256 (^{13}C, ω_1) × 256 (^{15}N, ω_2) × 4096 (^{1}H, ω_3) real points.

A three-dimensional HNCO experiment (Kay et al., 1990) was recorded in H_2O with 48 × 64 × 2048 complex points using sweep widths of 2265 Hz ($^{13}C'$, t_1), 1948 Hz (^{15}N, t_2), and 10,000 Hz (^{1}H, t_3), respectively. A modified 3D HACACO experiment (Powers et al., 1991) was recorded in D_2O with 18 × 44 × 2048 complex points using sweep widths of 2265 Hz ($^{13}C'$, t_1), 2656 Hz ($^{13}C^{\alpha}$, t_2) and 10 000 Hz (^{1}H, t_3), respectively. Solvent suppression was achieved using gradients (Bax & Pochapsky, 1992).

Three-dimensional ^{15}N-separated NOESY-HSQC experiments (Fesik & Zuiderweg, 1988; Marion et al., 1989b) were performed on the AMX500 spectrometer with mixing times of 50, 100, and 125 ms. Water suppression was accomplished using a spin-lock purge pulse as described by Messerle et al. (1989) combined with a homospoil pulse applied during the NOESY mixing times. The data were collected as 96 × 56 × 2048 complex points over sweep widths of 5682 Hz (^{1}H, t_1), 1624 Hz (^{15}N, t_2), and 8333 Hz (^{1}H, t_3) in 16 scans per increment for a total experiment time of approximately 120 h. The carrier position in the two ^{1}H dimensions was placed on the water frequency, and the ^{15}N carrier was set to 116.3 ppm. The processed data set sizes were 512 (^{1}H, ω_1), 256 (^{15}N, ω_2), and 4096 (^{1}H, ω_3) real points. A 3D ^{15}N-separated TOCSY-HSQC data set (Marion et al., 1989c) was collected using spectrometer conditions identical to the ^{15}N-separated NOESY experiments. A 28-ms clean MLEV mixing sequence (Griesinger et al., 1988) was used to effect ^{1}H–^{1}H magnetization transfer.

$^{3}J_{HNH\alpha}$ coupling constants were obtained from a modified version of the 3D HNHA-J experiment (Vuister & Bax, 1993). This sequence was modified by adding a 180° ^{15}N pulse immediately following the $^{1}H(t_1)$ evolution to facilitate the acquisition of a large number of ^{15}N increments with our (Bruker) pulse programmer. The data were collected in 16 scans per increments as 64 × 61 × 1024 complex points using 6250 Hz (^{1}H, t_1), 1623 Hz (^{15}N, t_2), and 8333 Hz (^{1}H, t_3) sweep widths, respectively. The coupling constants were obtained from the heights of the $^{1}H^{N}$ and $^{1}H^{\alpha}$ resonances as described by Vuister and Bax (1993). $^{3}J_{HNH\alpha}$ coupling constants were also measured in a high-resolution HMQC-J experiment (Kay & Bax, 1990). Identical ^{15}N and ^{1}H sweep widths were used as for the HNHA-J, with 400 t_1 increments resulting in a 246.4-ms acquisition time. The data were zero-filled in F_1 (^{15}N) to give a final digital resolution of 0.79 Hz/point.

Slowly exchanging amide protons were identified in a series of 20 2D ^{1}H–^{15}N HSQC (Bodenhausen & Ruben, 1980) experiments collected at 1.5–3-h intervals over a period of 64 h. Acquisition of the first experiment began within 5 min of dissolution of the protein sample in 100% D_2O buffer.

Table 1: Chemical Shifts for ^1H, ^{13}C, and ^{15}N Backbone Resonances of BHPTPase at 30 °C, pH 5.0[a,b]

residue	$^1H^N$	^{15}N	$^1H^\alpha$	$^{13}C^\alpha$	$^{13}C'$	residue	$^1H^N$	^{15}N	$^1H^\alpha$	$^{13}C^\alpha$	$^{13}C'$
A1			4.11	51.6	173.4	E80	8.24	116.4	4.05	59.6	179.3
E2	8.68	120.2	4.33	56.2	175.8	D81	7.87	120.8	4.58	58.3	177.4
Q3	8.49	121.6	4.37	55.3	175.2	F82	7.15	112.3	4.16	60.3	175.5
V4	8.26	122.3	4.13	62.0	175.6	V83	7.61	114.8	4.28	62.9	176.0
T5	8.05	118.9	4.36	61.5	173.9	T84	7.81	112.7	4.01	64.1	174.2
K6	7.88	125.1	4.51	54.7	174.4	F85	7.36	118.7	4.58	59.1	174.2
S7	8.70	113.2	6.23	55.9	173.5	D86	8.21	117.9	4.23	56.6	177.1
V8	9.38	121.1	5.37	59.1	168.9	Y87	7.81	115.7	5.01	56.8	173.9
L9	7.93	128.3	4.16	50.9	174.8	I88	8.98	122.9	4.72	60.4	173.5
F10	8.17	124.8	5.13	56.7	175.6	L89	8.19	125.1	5.49	51.7	176.0
V11	8.76	120.9	5.38	59.9	174.1	C90	9.26	118.4	6.23	54.8	174.8
C12	7.85	120.8	5.21	56.4	174.4	M91	7.35	114.9	5.01	56.6	176.3
L13	6.85	118.2	4.13	55.6	177.3	D92	7.77	116.7	4.96	52.2	174.7
G14	8.81	102.2	4.34, 3.85	45.1	175.1	E93			4.00	59.3	178.7
N15	9.25	120.2	3.95	54.7	171.4	S94	8.40	118.4	4.30	61.3	176.1
I16	7.89	103.7	4.78	62.9	176.6	N95	8.53	120.6	4.38	56.0	176.2
C17	9.24	118.9	5.03	59.2	174.5	L96	7.85	119.4	3.91	58.4	178.0
R18	9.76	119.1	3.78	60.7	177.3	R97	8.04	118.2	4.12	58.2	179.5
S19	10.18	116.9	3.85	64.0		D98	8.24	120.3	4.49	57.8	179.3
P20			4.18	65.2	179.9	L99	8.78	120.1	4.16	57.6	178.7
I21	6.84	116.9	3.79	65.1	175.5	N100	8.70	119.1	4.40	56.0	178.5
A22	8.00	121.9	3.13	55.6	176.4	R101	7.92	119.9	4.05	59.1	179.1
E23	7.93	114.0	3.37	58.6	176.6	K102	7.86	119.3	3.99	58.9	178.6
A24	7.25	119.6	4.13	54.7	180.5	S103	8.21	114.5	2.97	60.6	175.3
V25	8.47	119.4	3.49	66.3	177.3	N104	7.19	118.3	4.55	54.5	175.8
F26	8.63	121.9	3.79	62.8	176.4	Q105	7.59	115.0	4.29	55.6	175.2
R27	8.74	116.4	4.06	59.3	178.6	V106	7.41	118.9	4.18	61.0	175.1
K28	7.84	121.9	4.12	59.1	177.1	K107	8.52	125.8	4.12	57.5	176.6
L29	7.87	119.6	4.01	58.1	179.5	N108	8.49	116.0	4.60	52.6	173.6
V30	7.81	110.0	3.52	64.8	177.9	C109	7.88	118.2	3.87	60.1	174.1
T31	7.87	119.1	4.10	66.8	178.2	R110	8.50	127.9	4.48	56.4	175.9
D32	8.94	124.9	4.40	57.1	177.9	A111	7.71	123.2	4.24	53.2	177.3
Q33	7.43	114.5	4.30	55.5	174.4	K112	7.72	122.2	4.37	55.6	175.0
N34	8.02	115.0	4.70	54.5	175.3	I113	8.49	126.8	5.07	60.7	175.9
I35	8.13	109.2	4.91	60.7	177.1	E114	8.88	124.7	4.76	53.7	175.4
S36	7.97	117.9	3.99	61.7	175.9	L115	8.91	120.8	4.60	54.2	178.8
D37	8.62	118.3	4.59	55.7	176.2	L116	9.91	130.1	4.19	58.3	177.8
N38	7.95	115.5	4.84	53.2	173.2	G117				46.1	176.8
W39	7.70	118.8	5.59	56.8	175.6	S118	7.86	116.9	4.04	61.3	174.8
V40	9.20	125.7	4.41	62.9	174.9	Y119	7.96	118.2	4.18	61.6	175.6
I41	8.76	127.1	5.39	60.0	174.7	D120	7.42	119.4	4.53	52.7	177.6
D42	8.74	125.9	5.24	52.2	174.4	P121					
S43	8.96	113.7	5.40	57.7	171.4	Q122					179.2
G44	8.29	101.8	4.66, 3.08	44.6	170.5	K123	7.81	111.4	4.13	56.7	174.7
A45	9.08	118.1	5.19	49.0	178.3	Q124	8.18	120.2	4.67	54.5	173.9
V46	8.12	118.8	3.69	65.9	176.9	L125	7.23	121.8	3.63	57.9	
S47	7.95	112.7	4.59	57.1	174.1	I126			4.25*	58.0	175.5
D48	8.18	118.3	4.43	52.3	178.3	I127	7.78	128.8	4.22	61.0	174.9
W49	7.49	119.3	4.41	59.5	177.2	E128	8.90	127.4	4.15	56.2	177.1
N50	8.50	110.9	4.92	51.9	174.0	D129	8.72	123.9	4.31*	52.2	
V51	6.79	116.6	3.13	65.6	176.7	P130			4.62	62.6	176.0
G52	9.01	113.8	4.43, 3.59	44.9	174.2	Y131	7.78	122.2	3.98	62.3	177.3
R53	8.13	119.1	4.46	56.5	177.6	Y132	8.66	115.9	4.61	57.9	175.2
S54	8.61	118.9	4.93	58.5	169.5	G133	8.05	110.0	4.45, 3.96	44.0	173.2
P55			4.52	62.7	173.6	N134	9.17	119.2	5.28	50.9	176.3
D56	8.79	121.4	4.79	52.5	169.6	D135	8.44	117.6	4.44	58.6	178.9
P57			4.22	65.6	178.8	A136	8.40	123.1	4.27	55.2	180.1
R58	9.48	117.9	3.87	58.0	179.8	D137	8.04	118.3	4.61	57.7	178.7
A59	7.70	122.9	4.21	54.9	178.4	F138	7.84	118.6	3.76	63.0	176.3
V60	7.90	117.7	3.37	67.1	178.8	E139	7.77	120.4	4.60	58.4	178.4
S61	8.50	115.5	4.03	61.6	175.0	T140	8.35	118.3	3.95	67.2	175.9
C62	7.46	120.9	4.07	61.7	176.2	V141	7.68	120.7	3.84	66.5	178.2
L63	8.03	115.8	3.92	58.3	179.1	Y142	8.79	121.4	3.65	63.3	175.8
R64	8.52	121.3	4.07	59.1	180.6	Q143	8.62	117.4	3.62	58.4	179.9
N65	8.13	120.3	4.37	54.9	174.9	Q144	8.66	118.6	3.78	60.5	178.5
H66	7.49	115.3	4.74	54.6	173.9	C145	8.68	117.1	3.79	65.6	176.6
G67	7.96	107.8	4.08, 3.88	46.4	174.0	V146	8.40	120.6	3.14	67.5	177.3
I68	8.15	120.4	4.38	60.3	173.1	R147	7.38	115.0	4.02	60.1	180.4
N69	8.45	121.9	4.91	51.5	173.4	C148	8.44	115.9	3.94	63.7	176.7
T70	8.68	113.0	4.57	59.6	170.9	C149	8.93	116.0	3.97	65.0	176.0
A71	8.69	130.8	4.71	50.6	176.5	R150	7.85	117.7	3.89	59.8	177.8
H72	7.96	119.8	4.27	57.6	173.2	A151	7.22	120.6	4.28	54.9	180.0
K73	7.41	124.3	4.43	53.5	175.3	F152	8.42	120.1	3.75	60.7	176.1
A74	8.81	122.6	4.64	52.3	178.6	L153	7.86	117.4	3.72	57.3	178.0
R75	8.51	118.1	4.85	53.7	172.5	E154	7.53	114.3	3.92	58.4	178.0
Q76	9.02	123.1	4.72	54.5	175.6	K155	7.59	117.1	4.27	57.6	178.1
V77	8.87	125.8	4.10	63.0	175.5	V156	7.58	113.5	4.26	62.1	175.3
T78	9.61	120.1	4.80	59.3	175.1	R157	7.70	126.3	4.15	58.4	180.8
K79	8.64	118.1	4.12	59.8	178.1						

[a] ^1H chemical shifts are referenced to water (4.74 ppm). ^{13}C chemical shifts are referenced to TSP (0.0 ppm). ^{15}N chemical shifts are relative to NH_4NO_3 (119.4 ppm). [b] Tentatively assigned chemical shifts are indicated with asterisks.

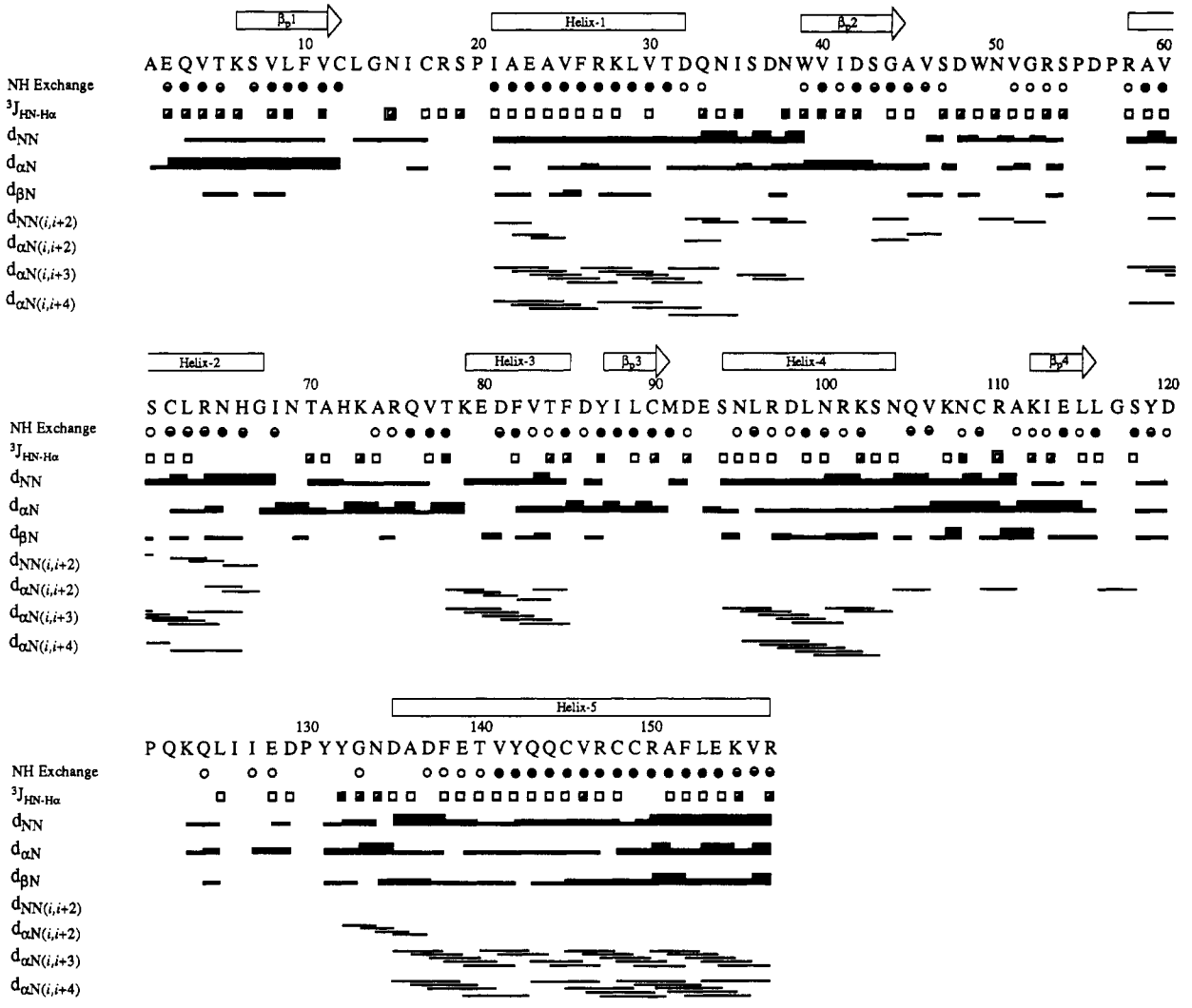

FIGURE 4: Summary of the NMR data used to characterize the secondary structure of the BHPTPase. Amide exchange rates: (solid circles) amides protected from exchange for 3 days in D_2O; (half-solid circles) amides with significantly reduced intensity after 3 days in D_2O; (open circles) amides observed after 1 h in D_2O; (no circles) fast exchange amides, not observed after 45 min in D_2O. $^3J_{HNH\alpha}$ coupling constants: (open squares) <5.5 Hz; (half-solid squares) 5.5–8.5 Hz; (solid squares) >8.5 Hz. β-Strand and α-helical secondary structure elements are indicated above the sequence. The sequential NOE intensities are represented by the thickness of the bar.

RESULTS AND DISCUSSION

NMR Assignments. The backbone ^1H, ^{13}C, and ^{15}N chemical shift assignments for BHPTPase were obtained by identifying the individual amino acid spin systems by amino acid type and sequentially linking the residues by correlating the ^{15}N and $^1H^N$ signals of the amides to the $^1H^\alpha$ and $^{13}C^\alpha$ signals of i and $i-1$ residues. To identify and assign the resonances of each amino acid spin system, a 3D ^{15}N-separated TOCSY-HSQC spectrum was recorded on [U-^{15}N]BHPTPase in which intraresidue correlations between the amide and side-chains protons for the different amino acid spin systems are obtained. Unfortunately, the relatively large size of BHPTPase limited the TOCSY transfer primarily to $^1H^N$–$^1H^\alpha$ correlations for the majority of the amino acids, thus preventing the unambiguous identification of the individual spin systems by amino acid type. Instead, this was accomplished using BHPTPase samples that were selectively ^{15}N-labeled by amino acid type. A total of 10 selectively ^{15}N-labeled BHPTPase samples were prepared, including ^{15}N-labeled lysine, valine, alanine, leucine, isoleucine, phenylalanine, tyrosine, aspartate, and glycine. Several of the selectively ^{15}N-labeled samples (e.g., [^{15}N]Lys, [^{15}N]Val, and [^{15}N]Ala) were labeled only at the desired amino acids, but others exhibited some degree of label scrambling due to transaminases (data not shown). In some cases, due to the known metabolic pathways of the amino acids, this scrambling of the ^{15}N label provided additional assignments by amino acid type (Muchmore et al., 1989).

In the next step of the assignment process, the individual amino acid spin systems were sequentially linked together using data obtained from 3D ^{15}N-separated NOESY-HSQC experiments. Figures 1 and 2 depict ^1H (ω_1), ^1H (ω_3) cross sections obtained from a ^{15}N-separated 3D NOESY-HSQC spectrum of [U-^{15}N]BHPTPase extracted at different ^{15}N amide frequencies (ω_2). The $^1H^\alpha$ and other aliphatic protons identified in the 3D TOCSY-HSQC experiment are indicated by boxes. As shown in Figure 1, strong sequential correlations were observed between $^1H^N(i)$ and $^1H^\alpha(i-1)$ of residues forming extended structures, and as illustrated in Figure 2, sequential $^1H^N$–$^1H^N$ NOEs are used to sequentially link residues involved in helical portions of the protein.

Analysis of the ^{15}N-separated NOESY-HSQC data provided sequential assignments for most of the amino acids participating in the regular secondary structure conformations (i.e., α-helix and β-strand), but sequential assignments for amino acids located in regions of nonregular secondary

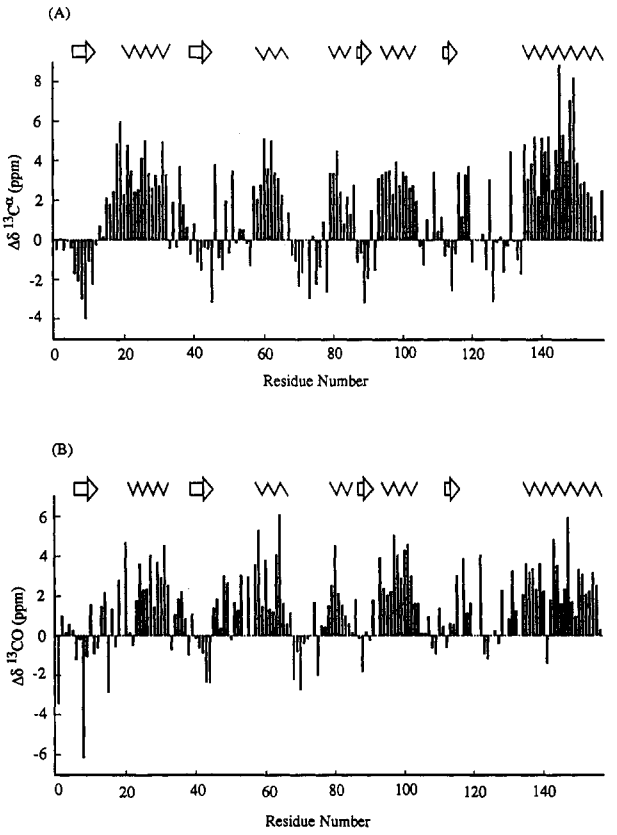

FIGURE 5: ^{13}C chemical shift deviations of BHPTPase from those of random coil (Richarz & Wüthrich, 1978; Spera & Bax, 1991): plot of $^{13}C^{\alpha}$ (A) and ^{13}CO (B) chemical shifts minus random coil values vs sequence number. The β-strand and helical regions as identified from NOE data are indicated by arrows and waves, respectively.

structure were lacking. In addition, assignment ambiguities were encountered due to overlapping ^{15}N and ^{1}H chemical shifts. To confirm and extend the sequential backbone assignments obtained in the NOESY data, 3D CT-HNCA and CT-HN(CO)CA triple-resonance experiments were performed on [U-^{15}N,^{13}C]BHPTPase. In the 3D HNCA experiment, amide ^{1}H and ^{15}N resonances are correlated with the $^{13}C^{\alpha}$ chemical shifts of the i and $i-1$ residues using scalar magnetization transfer steps which are largely conformation independent. Figure 3 shows $^{13}C(\omega_1)$, $^{1}H^{N}$ (ω_3) strips taken from a 3D HNCA experiment at the amide ^{15}N (ω_2) chemical shifts of residues R58–L63. Sequential assignments of the individual spin systems are obtained by comparison of the $^{13}C^{\alpha}$ chemical shifts as indicated in the Figure 3. However, for several residues, correlations with the $^{13}C^{\alpha}$ chemical shift of the $i-1$ residue were weak or missing. Ambiguities in identifying the $^{13}C^{\alpha}$ of the $i-1$ residue were alleviated by analyzing the data obtained from a 3D HN(CO)CA experiment (Figure 3). In the HN(CO)CA experiment, amide ^{1}H and ^{15}N resonances are correlated exclusively with the $^{13}C^{\alpha}$ chemical shift of the preceding residue by directing the magnetization transfer through the intervening carbonyl carbon. Comparison of the data obtained in the HNCA and HN(CO)CA experiments for each amide allowed the unambiguous assignment of $^{13}C^{\alpha}(i)$ and $^{13}C^{\alpha}(i-1)$ chemical shifts and facilitated the sequential linking of the amino acid spin systems. Confirmation of the backbone assignments was obtained by an analysis of 3D HNCO and HACACO spectra using the carbonyl chemical shift as the common frequency. This assignment procedure provided the complete sequential backbone ^{1}H, ^{13}C, and ^{15}N assignments for 147 of 151 non-proline residues in the BHPTPase (Table 1).

Secondary Structure. During the process of sequence-specific backbone resonance assignments, analysis of the ^{15}N NOESY-HSQC spectra yielded information about the secondary structure. The secondary structure of PTPase was determined on the basis of $^{1}H/^{1}H$ NOE data, $^{3}J_{HNH\alpha}$ coupling constants, amide proton exchange rates, and $^{13}C^{\alpha}$ and ^{13}CO chemical shifts. A summary of the data is given in Figures 4 and 5. The helices and β-strands are labeled according to their location in the protein sequence.

The helical regions of the protein were identified from NN(i,i+1), αN(i,i+3), and αN(i,i+4) NOEs, small $^{3}J_{HNH\alpha}$ coupling constants, and slow amide ^{1}H exchange rates (Wüthrich, 1986) (Figure 4). Furthermore, the $^{13}C^{\alpha}$ and ^{13}CO chemical shifts of residues identified as forming a helix were shifted downfield from the random coil values as shown in Figure 5 (Spera & Bax, 1991; Wishart et al., 1991, 1992). On the basis of these criteria, five helices were identified in the PTPase for residues I21–D32 (helix 1), R58–G67 (helix 2), K79–F85 (helix 3), S94–N104 (helix 4), and D135–R157 (helix 5). In the base of helix 3 (K79–F85), observation of nearly sequential αN(i,i+2) and αN(i,i+3) connectivities and a lack of αN(i,i+4) NOEs indicates that this region probably forms a 3_{10}-helix. Two α-helices (i.e., helix 1 and helix 2) start right after proline residues, as is commonly observed in many proteins.

As shown in Figure 4, the β-strands of PTPase contain residues K6–C12 (β_p1), W39–A45 (β_p2), Y87–M91 (β_p3), and K112–L116 (β_p4). The location of these strands was identified by strong αN(i,i+1) NOEs and weak or absent NN(i,i+1) NOEs, large $^{3}J_{HNH\alpha}$ coupling constants, and slowly exchanging amide protons (Wüthrich, 1986). The assignments of the residues in the β-strands were also supported by the $^{13}C^{\alpha}$ and ^{13}CO chemical shifts, which were mostly upfield relative to the random coil $^{13}C^{\alpha}$ shifts, as illustrated in Figure 5 (Spera & Bax, 1991; Wishart et al., 1991, 1992). The pairing of the β-strands to form the β-sheet was determined from long-range NOEs between the individual β-strands as shown in Figure 6. The NMR data indicate that PTPase consists of a four-stranded parallel β-sheet, with a $+1x$, $-2x$, $-1x$ folding topology. The strong interstrand NOE between $^{1}H^{N}$ of Y87 and $^{1}H^{\alpha}$ of V8 and the presence of several interstrand $^{1}H^{N}_{(i)}$–$^{1}H^{N}_{(j)}$ NOEs in the middle region of the β-sheet, e.g., $^{1}H^{N}_{Y87}$–$^{1}H^{N}_{S7}$ and $^{1}H^{N}_{Y87}$–$^{1}H^{N}_{L9}$, indicate that this four-stranded parallel β-sheet is not planar but may be twisted with closer contacts near the center of the sheet. The central β-sheet is composed of all hydrophobic amino acid residues (i.e., Y87-I88-L89 and V8-L9-F10-V11), and it is likely that this region forms the hydrophobic core of the protein. This β-sheet is further supported by amide proton exchange rates. Almost all amide protons of these hydrophobic residues located at the center of the β-sheet were well protected from exchange with solvent (Figure 4). A tentative hydrogen-bonding pattern between amide protons and carbonyl oxygens involved in the β-sheet consistent with the observed amide proton exchange data is indicated by dashed lines in Figure 6. In addition to the amino acids located in the β-sheet, many of the residues found in the helical regions such as I21–T31, L99, Y142–V146, and C148–C149 were also well protected from exchange.

CONCLUSIONS

Using a series of heteronuclear 3D NMR experiments, we have assigned the ^{1}H, ^{13}C, and ^{15}N backbone resonances of

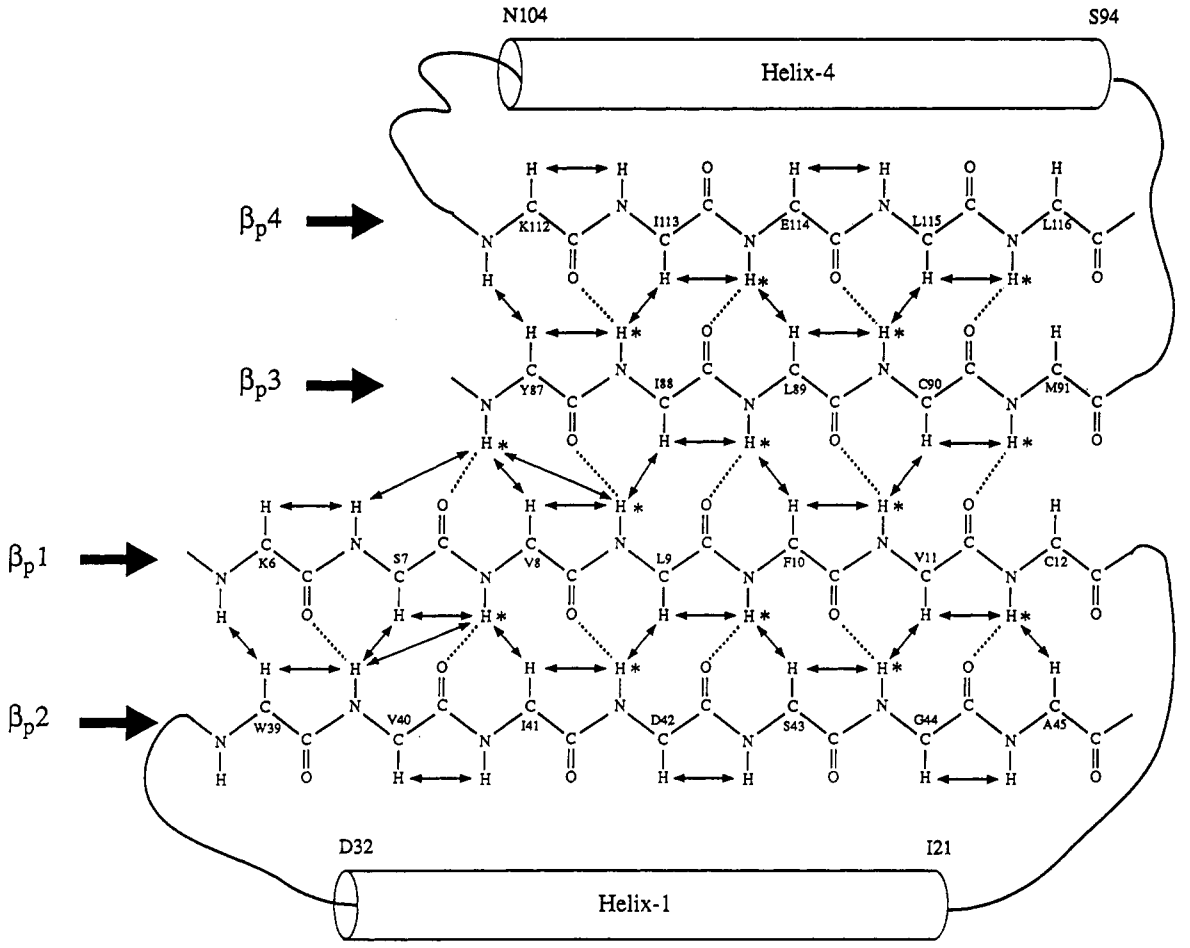

FIGURE 6: Central four-stranded parallel β-sheet secondary structure of BHPTPase. The observed NOEs that define this secondary structure are denoted by arrows, and tentative hydrogen bonds are indicated by dashed lines. The amide protons that were still present in the ^1H–^{15}N HSQC spectrum after incubation for 1 month in D_2O are marked by stars.

the low molecular weight bovine heart phosphotyrosyl protein phosphatase. In addition, from an analysis of NOE data, $^3J_{HNH\alpha}$ coupling constants, $^{13}C^{\alpha}$ and ^{13}CO chemical shifts, and amide proton exchange rates, the secondary structure of the protein was determined. The arrangement of the helices and β-strand structures in the protein revealed that the overall secondary structure topology of BHPTPase consists of two adjacent $\beta\alpha\beta$ units (Figure 6), which has been commonly observed in globular proteins (Rao & Rossmann, 1973; Richardson, 1976; Sternberg & Thornton, 1976; Nagano, 1977). The pattern of this parallel α/β organization is classified as a doubly wound parallel β-sheet, which is characterized by the presence of a twisted central β-sheet flanked on each side by a layer of helices and loops (Richardson, 1976; Sternberg & Thornton, 1976). The dominant organizing principle of parallel α/β proteins is the overwhelming right-handedness (much better than 99%) of $\beta\alpha\beta$ units. If we assume that this is also true for this protein, then it implies that helix 1 lies on the top of the β-sheet (Figure 6) and helix 4 is on the other side of the β-sheet. A definitive structural conformation awaits completion of side-chain assignments and a complete analysis of the NOE data. Further insight into the structure of BHPTPase is obtained by considering that in contrast to the hydrophobic–hydrophilic alternation shown by antiparallel β-strands, parallel β-strands are generally hydrophobic in their central portions and hydrophilic only at their ends (except for edge strands) (Lifson & Sander, 1979). These parallel β-strands are always buried on both sides in the protein, forming a hydrophobic core between sheet and helices.

Many of the kinetic and mechanistic features of this class of low molecular weight PTPases are well characterized. The phosphate monoester hydrolysis proceeds via a double-displacement mechanism involving the formation of a covalent phosphoenzyme intermediate, with the breakdown of this intermediate being the rate-limiting step in the catalytic pathway (Saini et al., 1981; Zhang & Van Etten, 1991). Recently, observation of the stoichiometrically trapped phosphoenzyme intermediate by ^{31}P NMR, together with site-directed mutagenesis studies of the BHPTPase, indicates that C12 is the enzymatic nucleophile (Wo et al., 1992a; Davis et al., 1992; 1994a; Cirri et al., 1993). Mutagenesis, kinetic, and ^1H NMR studies of human and bovine PTPases suggest that C17, R18, and H72 are also located at the active site of the enzyme (Zhou et al., 1993; Davis et al., 1994a,b). The secondary structure of BHPTPase obtained here appears to be in good agreement with these results. C12, the residue involved in the nucleophilic attack, is located at the C-terminal end of this four-stranded parallel β-sheet in close proximity to the other active-site residues, i.e., C17 and R18, that are in the loop region between the β_p1 strand and helix 1. This finding is consistent with the interpretation concluded on the basis of recent kinetic and mutagenesis studies that both R18 and, to a lesser extent, C17 play a structural role in aiding the proper orientation of the substrate phosphate moiety (Cirri et al., 1993; Davis et al., 1994a). The other active-site residue, H72, is located in the loop region after helix 2.

Low-Mr PTPase	V L F V C L G N I C R S P
Hs	I V F H C E F S S E R G P
Mm1	I V F H C E F S S E R G P
Mm2	V V F L C E F S S E R G P
XI	L I F H C E F S S E R G P
Dm	I I F H C E F S S E R G P
At	L I L H C E Y S A H R A P
Dd	I I F H C E F S S K R A P
Sp	L V F H C E H S A H R A P
Sc	L I I H C E F S S H R G P
CD45	I V V H C S A G V G R T G
HLAR	M V V H C S A G V G R T G
PTP 1B	V V V H C S A G I G R S G
VH1	V L V H C A A G V N R S G

FIGURE 7: Comparison of the active site region in the representative PTPases: sequence alignment of cdc25 homologs (Millar et al., 1991) from *Homo sapiens* (Hs), *Mus musculus* (Mm1 and Mm2), *Drosophila melanogaster* (Dm), *Xenopus laevis* (XI), *Arabidopsis thaliana* (At), *Dictyostelium disoideum* (Dd), *Schizosacchromyces pombe* (Sp), and *Saccharomyces cercevisiae* (Sc); CD45 (Streuli et al., 1989); HLAR (Streuli et al., 1988); PTP 1B (Gautier et al., 1991); VH1 (Millar et al., 1991).

The secondary structure of BHPTPase can also be used to further understand the chemical nature of the active site. Phenylarsine oxide (PAO) is known to be a powerful inactivating agent for enzymes that have "spatially close thiols" (Brown et al., 1987). It has been shown to inactivate some protein tyrosine phosphatases, including this family of PTPases. Active-site-directed inactivation of BHPTPase by PAO occurs slowly but with great affinity (Zhang et al., 1992). In a study of the sensitivity of cysteine mutations of BHPTPase, it was found that the rate of inactivation of BHPTP-C17A mutant was sharply reduced, indicating that C12 and C17 are spatially close thiols. Interestingly, it was also observed that a BHPTP-C90S mutant is inactivated 3-fold faster than the wild-type enzyme by PAO (J. P. Davis and R. L. Van Etten, unpublished observations), although kinetic studies indicated that this BHPTP-C90S mutant retains nearly the same enzymatic properties as the wild-type enzyme (Davis et al., 1994a). Our NMR data show that C90 is situated near the C-terminal end of the central $\beta_p 3$ strand, bringing it close to the active-site nucleophile C12 (Figure 5). This suggests that the C90 mutation may alter the local conformation of the β-sheet, thus resulting in enhancement of inactivation by PAO with C12 and C17 at the active site.

Despite the lack of significant sequence homology between this family of low M_r PTPases and the other cytosolic or receptor-like PTPases, all members of the PTPases appear to have an identical catalytical mechanism, namely that the hydrolysis reaction proceeds via the formation of a transient thiol–phosphate covalent intermediate (Guan & Dixon, 1991; Wo et al., 1992a; Cho et al., 1992). In addition to two essential residues in the conserved active site CXXXXXR motif, all of the PTPases contain a stretch of hydrophobic residues preceding the nucleophilic cysteine and a proline or glycine residue located after the arginine (Figure 7). This reveals the close resemblance of the chemical nature as well as the possible similarity of the local conformation at the active sites of the PTPases. Further structural comparisons await the three-dimensional structure determination of the protein tyrosine phosphatases. The backbone assignments that have been described here lay the groundwork for obtaining the side-chain assignments from 3D HCCH-TOCSY (Fesik et al., 1990; Bax et al., 1990) experiments. With the complete assignments, the 3D NOE data can be interpreted, allowing the three-dimensional structure of BHPTPase to be determined. This work, which is in progress, should aid in furthering our understanding of the mechanism and substrate specificity of the PTPases.

REFERENCES

Bax, A., & Ikura, M. (1991) *J. Biomol. NMR 1*, 99–104.

Bax, A., & Pochapsky, S. (1992) *J. Magn. Reson. 99*, 638–640.

Bax, A., Clore, G. M., & Gronenborn, A. M. (1990) *J. Magn. Reson. 88*, 425–431.

Bodenhausen, G., & Ruben, D. J. (1980) *Chem. Phys. Lett. 69*, 185–189.

Boivin, P., & Galand, C. (1986) *Biochem. Biophys. Res. Commun. 134*, 557–564.

Boivin, P., Galand, C., & Bertrand, O. (1987) *Int. J. Biochem. 19*, 613–618.

Brown, S. B., Turner, R. J., Roche, R. S., & Stevenson, K. J. (1987) *Biochem. 26*, 863–871.

Camici, G., Manao, G., Cappugi, G., Modesti, A., Stefani, M., & Ramponi (1989) *J. Biol. Chem. 264*, 2560–2567.

Chernoff, J., & Li, H. C. (1985) *Arch. Biochem. Biophys. 240*, 135–145.

Cho, H., Krishnaraj, R., Kitas, E., Bannwarth, W., Walsh, C., & Anderson, K. S. (1992) *J. Am. Chem. Soc. 114*, 7296–7298.

Cirri, P., Chiarugi, P., Camici, G., Manao, G., Raugei, G., Cappugi, G., & Ramponi, G. (1993) *Eur. J. Biochem. 214*, 647–657.

Davis, J. P., Zhou, M.-M., Wo, Y.-Y. P., Zhang, Z.-Y., & Van Etten, R. L. (1992) *American Society for Biochemistry and Molecular Biology Fall Symposium—Structure and Function of Protein Kinase and Phosphatases*, Keystone, CO, Oct 23–26, 1992, Abstract, p 99.

Davis, J. P., Zhou, M.-M., & Van Etten, R. L. (1994a) *J. Biol. Chem.* (in press).

Davis, J. P., Zhou, M.-M., & Van Etten, R. L. (1994b) *Biochemistry 33*, 1278–1286.

Dissing, J., Johnson, A. H., & Sensabaugh, G. F. (1991) *J. Biol. Chem. 266*, 20619–20625.

Driscoll, P. C., Clore, G. M., Marion, D., Wingfield, P. T., & Gronenborn, A. M. (1990) *Biochemistry 29*, 3542–3556.

Fesik, S. W., & Zuiderweg, E. R. P. (1988) *J. Magn. Reson. 78*, 588–593.

Fesik, S. W., Eaton, H. L., Olejniczak, E. T., Zuiderweg, E. R. P., McIntosh, L. P., & Dahlquist, F. W. (1990) *J. Am. Chem. Soc. 112*, 886–888.

Fischer, E. H., Charbonneau, H., & Tonks, N. K. (1991) *Science 253*, 401–406.

Gautier, J., Solomon, M. J., Booher, R. N., Bazan, J. F., & Kirschner, M. W. (1991) *Cell 67*, 197–211.

Griesinger, C., Otting, G., Wüthrich, K., & Ernst, R. R. (1988) *J. Am. Chem. Soc. 110*, 7870–7872.

Gu, M., York, J. D., Warshawsky, I., & Majerus, P. W. (1991) *Proc. Natl. Acad. Sci. U.S.A. 88*, 5867–5871.

Guan, K. L., & Dixon, J. E. (1990) *Science 249*, 553–556.

Guan, K. L., & Dixon, J. E. (1991) *J. Biol. Chem. 266*, 17026–17030.

Guan, K. L., Broyles, S. S., & Dixon, J. E. (1991) *Nature 350*, 359–362.

Heinrikson, R. L. (1969) *J. Biol. Chem. 244*, 299–307.

Hoffman, D. W., & Spicer, L. D. (1991) *Techniques in Protein Chemistry II*, pp 409–416, Academic Press, New York.

Hunter, T., & Cooper, J. A. (1985) *Annu. Rev. Biochem. 54*, 897–930.

Ikura, M., Kay, L. E., & Bax, A. (1990) *Biochemistry 29*, 4659–4667.

Kay, L. E., & Bax, A. (1990) *J. Magn. Reson. 86*, 110–126.

Lazaruk, K. D. A., Dissing, J., & Sensabaugh, G. F. (1993) *Biochem. Biophys. Res. Commun. 196*, 440–446.

Lifson, S., & Sander, C. (1979) *Nature 282*, 109–111.

Manao, G., Pazzagi, L., Cirri, P., Caselli, A., Camici, G., Cappugi, G., Saeed, A., & Ramponi, G. (1992) *J. Protein. Chem. 11*, 333–345.

Marion, D., Ikura, M., Tschudin, R., & Bax, A. (1989a) *J. Magn. Reson. 85*, 393–399.

Marion, D., Kay, L. E., Sparks, S. W., Torchia, D. A., & Bax, A. (1989b) *J. Am. Chem. Soc. 111*, 1515–1517.

Marion, D., Driscoll, P. C., Kay, L. E., Wingfield, P. T., Bax, A., Gronenborn, A. M., & Clore, G. M. (1989c) *Biochemistry 28*, 6150–6156.
McLaughlin, S., & Dixon, J. E. (1993) *J. Biol. Chem. 268*, 6839–6842.
Messerle, B. A., Wider, G., Otting, G., Weber, C., & Wüthrick, K. (1989) *J. Magn. Reson. 85*, 608–613.
Millar, J. B. A., McGowan, C. H., Lenaers, G., Jones, R., & Russel, P. (1991) *EMBO J. 10*, 4301–4309.
Muchmore, D. C., McIntosh, L. P., Russell, C. B., Anderson, D. E., & Dahlquist, F. W. (1989) *Methods Enzymol. 177*, 44–73.
Nagano, K. (1977) *J. Mol. Biol. 109*, 235–250.
Oakada, M., Owada, K., & Nakagawa, H. (1986) *Biochem. J. 239*, 155–162.
Olejniczak, E. T., & Eaton, H. L. (1990) *J. Magn. Reson. 87*, 628–632.
Powers, R., Gronenborn, A. M., Clore, G. M., & Bax, A. (1991) *J. Magn. Reson. 94*, 209–213.
Ramponi, G., Manao, G., Camici, G., Cappugi, G., Ruggiero, M., & Bottaro, D. P. (1989) *FEBS Lett. 250*, 467–473.
Rao, S., & Rossmann, M. (1973) *J. Mol. Biol. 76*, 241–256.
Richardson, J. (1976) *Proc. Natl. Acad. Sci. U.S.A. 73*, 2619–2623.
Richarz, R., & Wüthrich, K. (1978) *Biopolymers 17*, 2133–2141.
Rohan, P. J., Davis, P., Moskaluk, C. A., Kearns, M., Krutzsch, H., Siebenlist, U., & Kelly, K. (1993) *Science 249*, 1763–1766.
Ruggiero, M., Pazzagli, C., Rigacci, S., Magnelli, L., Raugei, G., Berti, A., Chiarugi, V. P., Pierce, J. H., Camici, G., & Ramponi, G. (1993) *FEBS Lett. 326*, 294–298.
Saini, M. S., Buchwald, S. C., Van Etten, R. L., & Knowles, J. R. (1981) *J. Biol. Chem. 256*, 10453–10455.
Spera, S., & Bax, A. (1991) *J. Am. Chem. Soc. 113*, 5490–5492.
Sternberg, M., & Thornton, J. (1977) *J. Mol. Biol. 110*, 269–283.
Streuli, M., Krueger, N. X., Hall, L. R., Schlossman, S. F., & Saito, H. (1988) *J. Exp. Med. 168*, 1523–1530.
Streuli, M., Krueger, N. X., Tsai, A. Y. M., & Saito, H. (1989) *Proc. Natl. Acad. Sci. U.S.A. 86*, 8698–8702.
Taga, E. M., & Van Etten, R. L. (1982) *Arch. Biochem. Biophys. 214*, 505–515.
Vuister, G. W., & Bax, A. (1993) *J. Am. Chem. Soc. 115*, 7772–7777.
Waheed, A., Laider, P. M., Wo, Y.-Y. P., & Van Etten, R. L. (1988) *Biochemistry 27*, 4265–4273.
Wishart, D. S., Sykes, B. D., & Richards, F. M. (1991) *J. Mol. Biol. 222*, 311–333.
Wishart, D. S., Sykes, B. D., & Richards, F. M. (1992) *Biochemistry 31*, 1647–1651.
Wo, Y.-Y. P., Zhou, M.-M., Stevis, P., Davis, J. P., Zhong, Z.-Y., & Van Etten, R. L. (1992a) *Biochemistry, 31*, 1712–1721.
Wo, Y.-Y. P., McCormack, A. L., Shabanowitz, J., Hunt, D. F., Davis, J. P., Mitchell, G. L., & Van Etten, R. L. (1992b) *J. Biol. Chem. 267*, 10856–10865.
Wüthrich, K. (1986) *NMR of Proteins and Nucleic Acids*, Wiley, New York.
Yarden, Y., & Ullrich, A. (1988) *Annu. Rev. Biochem. 57*, 443–478.
Yi, T., Cleveland, J. L., & Ihle, J. N. (1992) *Mol. Cell. Biol. 12*, 835–846.
Zhang, Z.-Y., & Van Etten, R. L. (1990) *Arch. Biochem. Biophys. 228*, 39–49.
Zhang, Z.-Y., & Van Etten, R. L. (1991) *J. Biol. Chem. 266*, 1516–1525.
Zhou, M.-M. (1993) Ph.D. Thesis, Purdue University, W. Lafayette, IN.
Zhou, M.-M., Davis, J. P., & Van Etten, R. L. (1993) *Biochemistry 32*, 8479–8486.
Zuiderweg, E. R. P., & Fesik, S. W. (1989) *Biochemistry 28*, 2387–2391.